A PERMANENT MAGNET PHASE SHIFTER FOR THE EUROPEAN X-RAY FREE ELECTRON LASER

H. H. Lu, M. T. Wang, J. Zhuang, D. Wang
Institute of High Energy Physics, Chinese Academy of Sciences
19B Yuquan Lu, Shijingshan District, Beijing, 100049, P. R. China
B. Faatz, Y. Li, J. Pflueger
Deutsches Elektronen Synchrotron, DESY, Notkestr 85, 22603 Hamburg, Germany.

Abstract

In undulator systems with adjustable gaps phase shifters are needed to exactly control the phase retardation between electrons and the radiation field over the entire length of an undulator system. A phase shifter based on Permanent Magnet technology for the use in the European XFEL has been developed and tested. Specifications are given. This paper will explain its magnetic principle and design. Magnetic test results are presented and thoroughly discussed. Special attention is given to the operation in the XFEL.

1. INTRODUCTION

The European X-Ray Free Electron Laser (XFEL) will be a user facility covering the wavelength range from 0.1 to 1.6 nm [1]. High power radiation will be generated using Self-Amplified Spontaneous Emission (SASE) [2, 3]. Saturation requires typical undulator system lengths of about 200m. At the XFEL the radiation wavelength can be changed by changing either the electron beam energy or the undulator gap.

Long undulator systems cannot be built as one contiguous device. They need to be segmented. There are two reasons to do so: First, mechanical manufacturing of very large devices becomes more and more difficult and expensive if not impossible at all. Second, in order to keep the electron beam properties well under control, additional components are needed in regular intervals such as quadrupoles, beam position monitors, synchrotron radiation absorbers, vacuum pumps etc. In addition a phase shifter, the subject of this paper, is required. These components are placed in intersections in between adjacent undulator segments.

A reasonable compromise has been found for the XFEL. Undulator segments will be 5m long, followed by a 1.1m long intersection [1]. The combination of an undulator segment and an intersection is called an undulator cell.

When the gap is changed in such an undulator system the radiation wavelength changes accordingly and the phase advance between electrons and the photon field changes too. For one gap phase matching can be obtained by matching the length of the intersection to the radiation wavelength. This is used in fixed gap undulator systems such as FLASH or LCLS [4, 5]. For systems with variable gap, however, an additional variable phase delay is needed to provide proper matching between individual undulator segments.

A phase shifter can be made using a chicane consisting of three electro magnets (EMs). This approach was made in an early design study for the XFEL [6, 7]. There are, however, four aspects to be considered using EM phase shifters: First, they require a substantial amount of space. Second, EM phase shifters are difficult to adjust and need trim coils in order to avoid any un-wanted beam steering. This may slow down the gap adjustment speed of an undulator system using many phase shifters significantly. For example the SASE2 system of the XFEL consists of up to 42 cells requiring 41 phase shifters [1]. Third, since the length of an intersection is limited and it is densely packed, the fringe field of the chicane magnets might interfere with other components such as the field terminations plates of the undulator segment or the quadrupoles. And finally, fourth, EM systems dissipate heat, which could be a problem to the stringent temperature stability requirements in XFELs [1].

This paper concentrates on a novel permanent magnet (PM) design of a phase shifter, which is intended to be used in the XFEL. First ideas were presented in ref [8] and results obtained from a prototype were introduced in [9]. This paper gives a comprehensive overview over the design and the choice of parameters. Results of magnetic measurements are presented. Modes of using and operating such device in the undulator systems of the XFEL are discussed in detail.

2. Design Considerations

Basics

The retardation of the ponderomotive phase of an electron with respect to the radiation field of radiation wavelength, λ_R, can be expressed as [10]:

$$\varphi(z) = \frac{2\pi}{\lambda_R}\left\{\frac{z}{2\gamma^2} + \frac{1}{2}\int_{-\infty}^{z} x'^2\,(z')dz'\right\} \tag{1}$$

Here z is the coordinate along the beam path, γ is the electron velocity in units of its rest mass (0.551 MeV) and x' is the electron deflection angle. Eq. (1) assumes forward direction i.e. along the electron beam axis. x' can be derived from the magnetic field distribution along the beam axis, $B_y(z)$, by:

$$x'(z) = \frac{e}{\gamma mc}\int_{-\infty}^{z} B_y(z')dz' \tag{2}$$

Here e is the electron charge, m its mass and c the velocity of light.
These relations are quite general. In practice the integration is extended only over regions with non-zero magnetic field. For all intents and purposes of this paper the integration can be restricted ±200mm without any sacrifice on accuracy. The origin of the z coordinate is arbitrary. In this paper it is at the beginning of the intersection.

The first term of Eq. (1) describes the phase advance in free space. The second represents the additional contribution of the magnetic field of the phase shifter to the phase delay. The phase change due to field only is given by:

$$\Delta\varphi(z) = \frac{2\pi}{\lambda_R 2\gamma^2}\cdot\left(\frac{e}{mc}\right)^2 \int_{-\infty}^{z}\left(\int_{-\infty}^{z''} B_Y(z')dz'\right)^2 dz'' = \frac{2\pi\ n}{\lambda_U\left(1+0.5K_U^2\right)}\cdot\left(\frac{e}{mc}\right)^2 \left\{\int_{-\infty}^{z}\left(\int_{-\infty}^{z''} B_Y(z')dz'\right)^2 dz''\right\} \tag{3}$$

Here the radiation wavelength of a planar undulator was expressed by:

$$\lambda_R = \lambda_U\left(1+0.5K_U^2\right)/n2\gamma^2 \tag{4}$$

where n is the number of the harmonic and K_U the undulator parameter is defined as.

$$K_U = \frac{e\lambda_U B_U}{2\pi\ mc} \tag{5}$$

λ_U and B_U are the undulator period length and peak field, respectively. For the SASE undulator systems of the XFEL only the first harmonic is of interest, so n=1. In the second form of Eq. (3) electron energy is eliminated.
The properties of B_U determine the performance of the device. A proper magnetic design does not only guarantee the required parameters, minimizes unwanted field errors. In this case only the total phase shift is of interest. It is obtained from Eq. (3) by extending z to $+\infty$. The Phase Integral, PI, is defined as:

$$PI = \int_{-\infty}^{\infty}\left(\int_{-\infty}^{z''} B_Y(z')dz'\right)^2 dz'' \tag{6}$$

In order to vary PI the strength of B_Y must be adjustable. In a PM device this is accomplished through changing the gap. In an EM device the excitation current through a coil is altered.

Magnetic Design Principle

Boundary conditions for the phase shifter were set by general considerations and by special requirements. There is a number of components to be placed in an intersection such as end corrector trim coils for the undulator, a synchrotron radiation absorber, a re-entrant cavity beam position monitor, a quadrupole on a movable support, the phase shifter, a vacuum getter pump, vacuum flanges etc. Since the available length for the intersection was 1.1m. This required some dense packing of components: As a result there were five prerequisites for the XFEL phase shifter:

1. In order to keep design and production effort low there should be only one standard phase shifter for the XFEL undulator systems. Its parameters will be chosen such that it covers all needs.
2. The phase shift should be controlled by one single parameter. Consequently all field errors must be small enough so that they can be neglected. Consequently the device must be completely neutral to the beam and no deflection or offsets in the horizontal and vertical direction must occur when the phase is changed.
3. Stray field need to be minimized in minimize interference with other magnetically active elements.
4. The available total length for the intersection of 1.1m restricts the length of the phase shifter to a maximum of 230mm.
5. Any heat dissipation should be avoided or minimized so that the temperature stability of the undulator system is not affected.

A PM solution for these requirements was developed. The magnetic design principle is illustrated in Fig. 1a). The whole magnetic system is encaged in a double E-shaped rigid soft iron zero potential yoke. The gap between the top and bottom yoke is called the yoke gap as shown in Fig 1 a). It chosen to be 10mm and cannot be changed. The yoke is kept at zero potential it therefore very effectively terminates and confines any fields to the inside.

Outside the phase shifter the field contribution is ideally zero. Inside the yoke there are four magnetic arrays, two in the top and two in the bottom. They are moved synchronously in order to vary the field and therefore the phase integral. Their position is characterized by the magnet gap in Fig.1a). Each of the four arrays consists of two poles, one full and two half magnets. There is a high degree of symmetry in the magnetic structure. On going from the left, the first pole has a negative sign, followed by a positive pole. The half on the right hand side is mirror symmetric to the left hand side. For symmetry reasons the total field cancels at any gap. However, if its thickness is too small, the iron yoke in the centre might perturb the symmetry and deteriorate field integral cancellation.

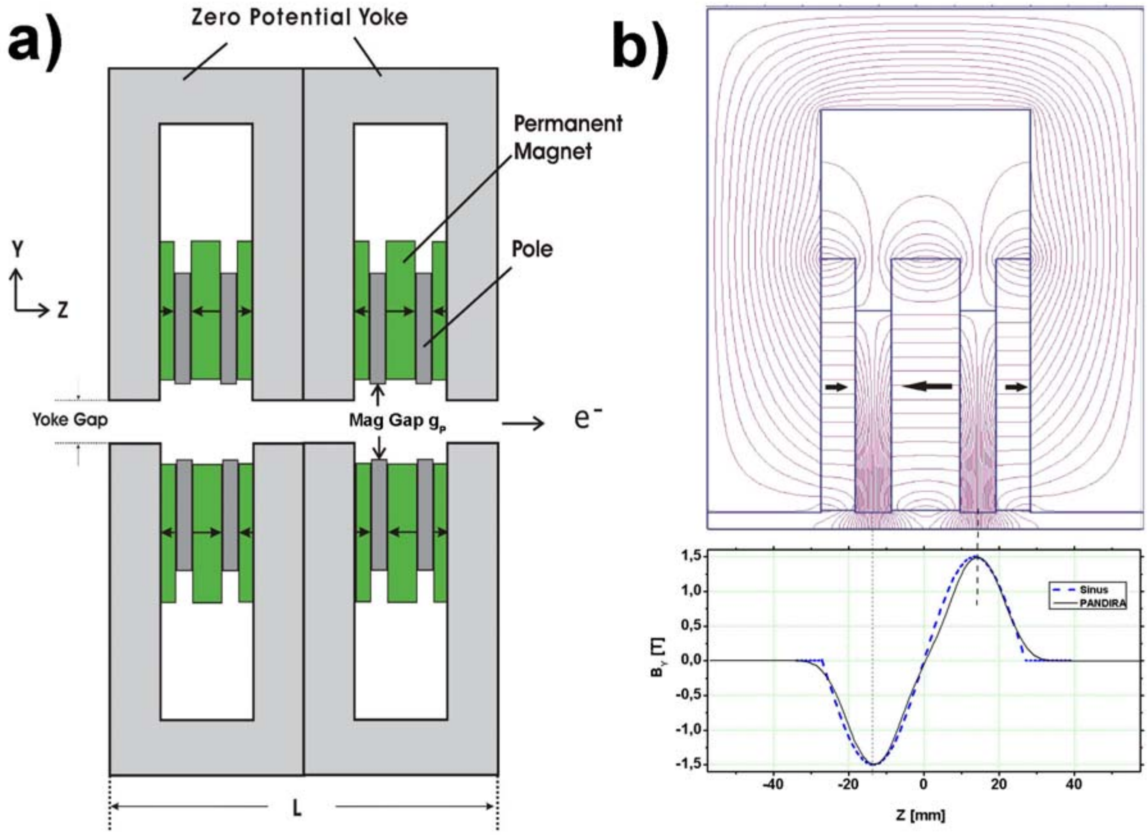

Figure 1:

a) Magnetic design principle of the Phase Shifter. Poles and magnets move symmetrically inside the zero potential soft iron yoke. This yoke is kept fixed and does not move. Positive and negative poles are in a geometrically identical environment so that there is no net first field integral.

b) Top: 2-D Flux line plot of 1/4 of the full geometry shown in a). The magnet gap is 10mm and corresponds to the maximum strength. Bottom: The full line represents the field distribution along the symmetry axis. The approximation by a single sinusoid is shown by the dashed line.

The upper part of Fig. 1b) shows a 2-D Flux line plot of ¼ of the structure shown in Fig. 1a). It was generated using PANDIRA [11]. It nicely demonstrates the above requirements: There are no flux lines entering or leaving the yoke in the gap region, where the field is consequently very low. The symmetry of both poles can be seen by following any flux line crossing the gap. It crosses the gap twice but with opposite sign, so that there is no net contribution to the field integral. The field distribution along the axis is shown by the full curve in the lower part of Fig. 1b). The field under the iron yoke is practically zero. The dashed line field is an analytical approximation using a single sinusoid with a period length of twice the pole distance, dashed line. Thus the full field distribution of the phase shifter shown in Fig. 1a) is therefore a double sinus function. It is shown in Fig 2 a), full line. It can be expressed analytically by:

$$B_y(z) = \left\{ B_P \sin\left(\frac{2\pi(|z| - \Delta P/2)}{\lambda_P}\right) \right\} \quad \text{for} \quad \frac{\Delta P}{2} \le |z| \le \left(\lambda_P + \frac{\Delta P}{2}\right) \tag{7}$$

B_y is zero outside. In the example in Fig 2 λ_P, and ΔP are both 50mm, the resulting peak field, B_P, is about 1.5T. This arrangement will be called double sinus field. The suffix ‘P’ denotes phase shifter parameters. The double sinus field configuration has an advantage as compared to that of a conventional undulator. This is demonstrated in Fig. 2a) as well. Here a comparison is made between the double sinus field distribution and that of a conventional undulator with a Cosinus like field with the same field strength but proper half pole termination. It can be expressed by:

$$B_y(z) = \left\{ B_P \cos\left(\frac{2\pi|z|}{\lambda_P}\right) \right\} \text{ for } |z| \le \frac{N\lambda_P}{2} \quad (8)$$

Again B_y is zero outside. Here N is the number of periods, N=2 in Fig.2. For simplicity and easier comparison, half poles with full strength and a step termination are assumed. As can be seen in Fig. 2a) the areas under the full and dashed curves are identical. However, since there are no half poles, the double sinus field leads to a larger 1st Integral excursion than the Cosinus type field. This is seen in Fig 2 b). Fig 2 c) shows the integrand inside the curled brackets in Eq. (3). Finally Fig 2 d) shows the evolution of the phase integral along z. It is seen that for the double sinus field the value saturates at a 21450 T^2mm^3 and 7150 T^2mm^3 for the sinus field and Cosinus-type field, respectively. Thus the same amount of magnet material results in a three times larger phase shift if arranged in the double sinus configuration. Using Eqs (7) and (8) an exact analytical evaluation of eq. (6) leads to:

$$PI_{Double\ Sinuns} = \frac{3\ B_P^2 \cdot \lambda_P^3}{4\pi^2} \quad (9)$$

for the double sinus field and

$$PI_{Co\sin us} = \frac{B_P^2 \cdot \lambda_P^3}{4\pi^2} \quad (10)$$

for the Cosine like field. Here the factor 3 in the phase integral is evident.

Once the geometry of the PM phase shifter is defined *PI* in Eq. (9) depends only on the gap, g_P, of the phase shifter.

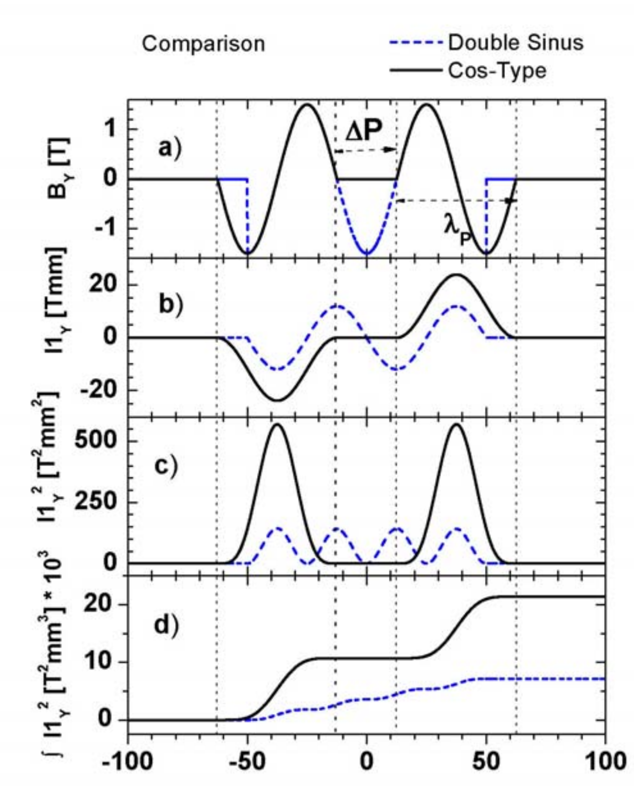

Figure 2: Comparison of the double sinus field configuration with a conventional Cosinus type field as used in undulators. The Phase Integral as defined in Eq.(6) is the value at z=100 in d). For more details see text.

3. Choice of Parameters, Specifications

In this section a detailed discussion of specifications and device parameters is given. Even without specific reference Table 1 gives a summary.

Tuning Range

One problem of wavelength tune-ability is sketched in Fig. 3. Here two undulator segments separated by a distance L, the length of the intersection are shown. Two cases need to be distinguished:

a) The field of an undulator segment has even symmetry i.e. it is mirror symmetric with respect to the undulator center. Therefore it has an odd number of poles and both end poles have the same polarity. This case is shown in Fig.3a). In this example there are 9 periods with 19 poles. The end poles of two adjacent segments always have the same polarity.

b) The field of an undulator segment has odd symmetry i.e. it is anti-symmetric with respect to the undulator center. Therefore it has an even number of poles and the end poles have opposite polarity as shown in Fig3b). This example has 9½ periods with 20 poles. In gap tune-able systems odd symmetry has an advantage since gap dependent errors of the two ends mutually cancel. The end poles of two adjacent end poles always have opposite polarity.

The condition for the phase advance over the intersection from end pole to end pole is $\varphi(L) = \nu\,\pi$. ν is called the Phase Number. For even symmetry like in Fig 3a) ν is even, ν= 2,4,6… For odd field geometry as shown in Fig.

3b) ν is odd, ν=1,3,5… For a complete undulator cell consisting of one segment plus one intersection the total phase advance is always an even multiple of 2π in both cases. Using eq. (1), (3) and (6) the phase matching condition is:

$$PI(g_P) = \left(\frac{mc}{e}\right)^2 \left(\frac{\lambda_U\left(1+0.5K_U^2(g_U)\right)}{2\pi\ n}\nu\ \pi - L\right) = \left(\frac{mc}{e}\right)^2 (\lambda_R \gamma^2 \nu\ - L) \geq 0 \qquad (11)$$

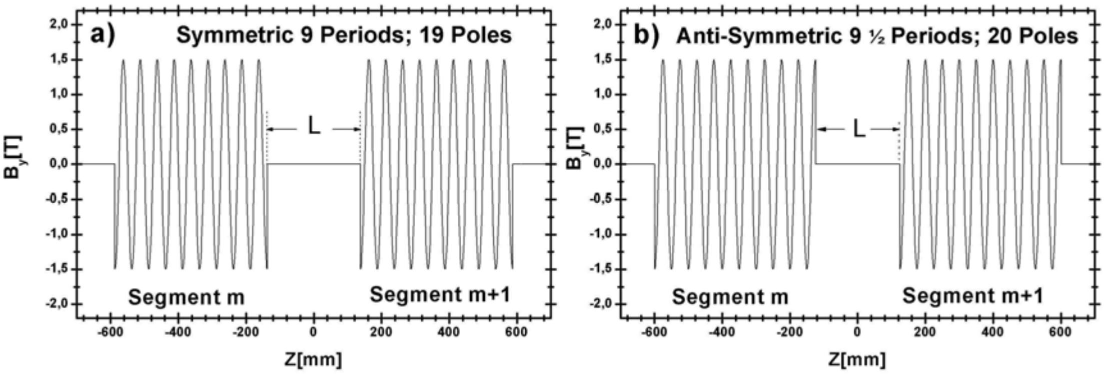

Figure 3: Two undulator segments separated by an intersection distance L: a) Symmetric Undulator field, both end poles have same sign. b) Anti-symmetric Undulator, end poles have opposite sign

The suffix 'U' distinguishes the properties of the undulator segment from that of the phase shifter denoted by the suffix 'P'. For a given undulator gap, g_U, eq.(11) can be used to determine the gap of the phase shifter, g_P, to obtain the required phase integral. The inequality on the right hand side emphasizes the fact, that the Phase integral is always positive and a phase shifter can only create additional, positive phase delay.

Depending on the field geometry, the Phase Number, ν, has to be the at least the next nearest even/odd number fulfilling the condition:

$$\nu \geq L / \lambda_R \gamma^2 \qquad (12)$$

Although ν can be chosen arbitrarily the required Phase Integral increases with increasing ν. For wavelength tune-able systems there is an aspect, which is illustrated in Fig 4. Here the Phase Integral for XFEL wavelengths marking the tune-ability ranges from 0.1 to 0.4 and 0.4 to 1.6nm is plotted as a function of the Phase Number, ν, according to Eq. (11). For 0.1nm ν ≥10 is required in order to have a positive Phase Integral. There is only moderate Phase Integral required to obtain this value. At 0.4nm ν can be as small as 3. For a given ν, there is a disruption at wavelength given by:

$$\lambda_R = \frac{L}{\nu\ \gamma^2} \qquad (13)$$

For shorter wavelengths the Phase Integral becomes negative. Then the phase shifter has to be adjusted to a larger ν value. Choosing ν large enough avoids this discontinuity over the wavelength range but in turn requires an appropriately large tuning range for the Phase Integral.

For the XFEL undulator systems the final decision weather to use odd or even field symmetry in the undulator systems has not yet been made, so that both options are kept open.

The worst case is at SASE3, which requires tuning from 0.4 to 1.6nm. Here a maximum Phase Integral of about 25000T^2mm^3 is planned: This allows contiguous tuning at ν=3, 4 and 5.

For SASE2 contiguous tuning is possible for ν≥10.

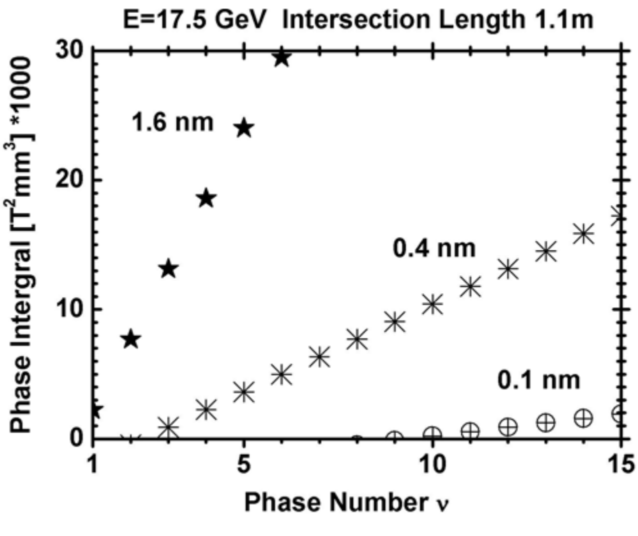

Figure 4: Required Phase Integral for different radiation wavelength as a function of the Phase Number

Adjustment Accuracy

An adjustment error of a phase shifter results in a mismatch of the ponderomotive phase between different segments, which in turn results in a reduction of FEL power. The most prominent source for this error is the limited adjustment accuracy of the phase shifter gap control. Knowledge of the required accuracy helps to keep the effort for the motion control within reasonable limits. This aspect becomes even more important for large undulator systems using many phase shifters. In a first step the FEL code GENESIS 1.3 [12] was applied in order to get study the requirements on phase adjustment accuracy. This work was a continuation of an earlier study [13]. Phase mismatch errors were statistically distributed over the cells of an undulator system. Homogeneous random distributions were assumed. The widths of these distributions were chosen to be ±5, 10, 20, 30, 40, 50 and 60°. For each width 20 different configurations were calculated in order to get some statistics. For each configuration the optical phase shake as described in [13] and the FEL power using GENESIS 1.3 was calculated. Each configuration results in one data point. The results are shown in Fig. 5. It is seen that a phase match errors of ±5° leads to a negligible power reduction, which is hard to distinguish from the statistical scatter of the data. An error of ±10°, however, leads to a power reduction of less than 10%, which is clearly visible. Even a large fraction, but not all, of the ±20° configurations show power reduction levels below 10%. Although this threshold is somewhat arbitrary it is large enough to be safely distinguished from the statistical scatter in the data. Larger phase match errors show correspondingly higher power reduction. As a conclusion a phase match error of ±10° is considered acceptable.

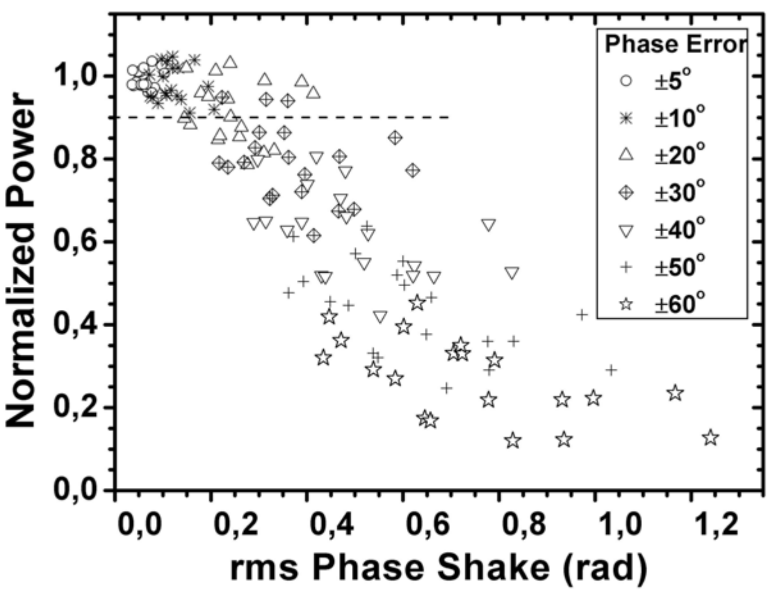

Figure 5: Normalized FEL power and RMS Phase shake for different widths of phasing errors.

For an estimate on the required gap adjustment accuracy the gap dependence of the Phase Integral is needed. An easy analytical estimate can be obtained in the following way:

The iron yoke of the phase shifter sets Neumann boundary conditions (field lines perpendicular to the iron surface). See also Fig. 1. Magnetically the situation of this geometry is fully equivalent to that found in a Halbach type Hybrid Undulator. The gap dependence can therefore be described with an exponential of the form:

$$B_Y = a \ \exp\left(b \ (g/\lambda_P) + c(g/\lambda_P)^2\right) \qquad (14)$$

Values for *a*, *b* and *c* were taken from ref. [14]. For the period length, λ_P=55mm is assumed. Then the Phase Integral and its derivative is easily calculated using eq. (9) and (14).

This estimate is rather conservative in the sense that it rather over- than underestimates the field and its derivatives leading eventually to slightly tougher requirements.

The worst case requirement is for the SASE3 case, when it is operated at λ_R=1.6nm. At ν=5 this requires the full Phase Integral of about 25000T^{2}mm^3 corresponding to smallest gap with largest derivative, see Fig. 4. In this case the gap needs to be adjusted to better than ±50μm for a phase jitter tolerance of 10° (0.175rad). At shorter wavelengths the requirements on gap adjustment is looser since a smaller Phase Integral correction is needed.

For SASE2 operated at ν=11 a Phase Integral of only about 10000T^{2}mm^3 is required, see Fig. 4. The reduced gap derivative of the Phase Integral counteracts the shorter radiation wavelength, so that the gap tolerance is approximately unchanged. At 0.1nm the gap tolerance is further relaxed.

Field Integral Tolerances

Field integral tolerances were estimated relative to electron beam size and divergence. As compared to the photon sizes this is the worst case, see Table 5.2.2. of ref. [1]. In the XFEL undulator sections the RMS beam divergence is typically in the range of 1-2 μrad and the beam RMS size in the range of 20-30μm. Any field integral error must not larger than 5% of the smaller of these values. The resulting requirement for the first field integral is only 0.004Tmm, which is not only a challenge for the performance but for the accuracy of magnetic measurements as well. The error budget for the second field integral is 67 Tmm^2, which is easier to achieve.

Table 1 Specifications and resulting design parameters of the phase shifter

Specifications		
Device length	[mm]	≤230
Min. Gap	[mm]	10
Max. Gap	[mm]	> 100
Max. total 1st Field Integral error	[Tmm]	0.004
Max. total 2nd Field Integral error	[Tmm^2]	67
Required max. Phase Integral	[T^2mm^3]	25000
Phase adjustment accuracy	[°]	±10 (0.175 rad)
Gap control accuracy	[μm]	±50
Device Parameters		
Full Magnet Size (Length × Width × Height)	[mm^3]	18 x 75 x 75
Half Magnet Size (Length × Width × Height)	[mm^3]	9 x 75 x 75
Magnet Material		NdFeB
Remanent Field @ 20°C	[T]	≥ 1.26
Coercive Field, $H_{C,J}$ @ 20°C / 60°C	[kA/m]	1670 / 1190
Pole Size (Length × Width × Height)	[mm^3]	9.5 x 60 x 60
Pole Material		FeCo, annealed at 850°C
Saturation Polarization	[T]	> 2.35
Coercive field	[A/m]	< 240
Phase Shifter Period Length, λ_P	[mm]	55
Yoke Material		ARMCO Soft Iron annealed at 850°C
Saturation Polarization	[T]	2.15
Coercive Field (annealed)	[A/m]	70
Yoke Thickness	[mm]	30

Magnet Parameters

The parameters and dimensions of magnetic parts were determined using RADIA [15] and PANDIRA [11], see also Fig.1 b). The resulting dimensions are listed in Table 1 too. The bottom part of Fig.1b) shows the calculated field of the phase shifter with a gap of 10mm. Here a peak field of 1.5T is obtained. It can be described by a single sinusoid with a period length of 55mm, which corresponds to the lengths of poles and magnets given in table 1.

4. Results

Mechanics

A prototype phase shifter following these requirements has been built. It is shown in Fig. 6. Its total overall height is 1150mm, that of the iron yoke is 700 mm. Its total length is 230mm. As explained in Fig. 1 the yoke, which circumvents the magnetic parts is rigidly fixed to the backing plane. In order to change the magnetic gap a double translation stage with a right/left handed spindle is used. In this way only one single MAXXON servo motor drive system is sufficient to control the magnetic gap. It is seen in the upper part in Fig. 6. For simplicity of

Figure 6: Prototype Phase shifter

the system, the gap position is determined by the spindle rotation using the values of the motor controller. The accuracy of this method is illustrated in Fig. 7. Here an external dial gauge with ±1µm accuracy is used It measures the motion of one half (half gap). Twice this value is compared with the reading of the motor controller. The difference of this measurement is shown as a function of the dial readings. The travel of the micrometer dial is limited to 10mm. Therefore tests were restricted to the gap range of 10-30mm, where magnetic forces are high and to 110-130mm, where they are negligible.

The mechanical deformation of the magnet support system at high magnetic forces at low gap leads to a deviation of about 100µm. This deviation vanishes as the gap is increased. It is also visible on the vanishing slope. In addition there is a systematic difference depending on the direction of movement. This hysteresis amounts to 100µm and is due to mechanical play, back lash, elasticity and friction of the magnet systems in the iron yoke and in the guiding system. Three closed loop cycles open →close →open are shown in Fig. 7. The measurements are very reproducible and coincide within line width, typically to ±1µm, the accuracy of the dial. Thus the mechanical deformation neither influences reproducibility nor absolute accuracy if the direction of motion is taken into account.

If, however, the gap is mover back and forth, i.e. the direction of motion is not considered, the mechanical hysteresis leads to a position error of ±50µm. This error is acceptable for operation within the phase adjustment accuracy of ±10° as explained above. ´

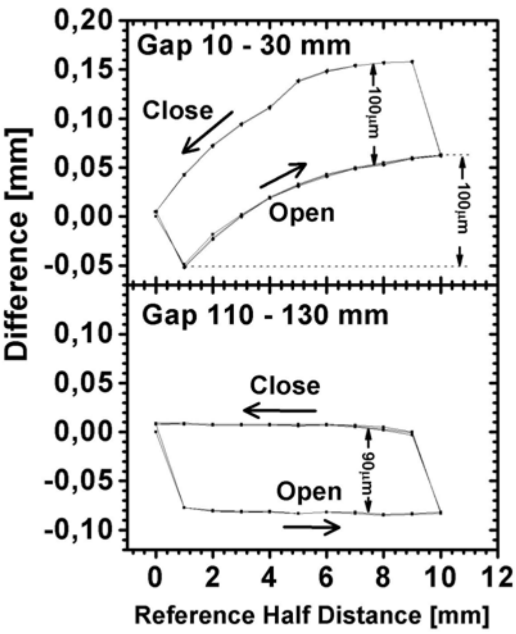

Figure 7: Difference of twice the half gap reading to that of the motion controller. The half gap was measured by an external micrometer. The range of this device was 10mm, limiting the gap range to 20mm. Two sets of measurements one at small and one at large gap was made. Three full cycles are shown. All coincide within line width. There is a deviation between the open and close direction (hysteresis) of 90-100µm. The curvature at small gaps results from mechanical deformation of up to 100µm due to magnetic forces. It rapidly fades off with increasing gap. At large gaps there is no deformation and the line is straight.

Magnetic Measurements

Results of magnetic field measurements at a magnetic gap of 10mm are shown in Fig. 8. The vertical B_Y field profile is shown in Fig 8a). A peak field of 1.49T can be observed. Note the symmetric field shape of positive and negative poles. The field can be described well by a single sinusoid. In the left part of Fig. 8a) a corresponding fit with λ_P = 54.6mm and ΔP=56.6mm is shown. Both values correspond well with the geometry of the device. For λ_P 55mm and for ΔP 60mm are expected. See Table 1.

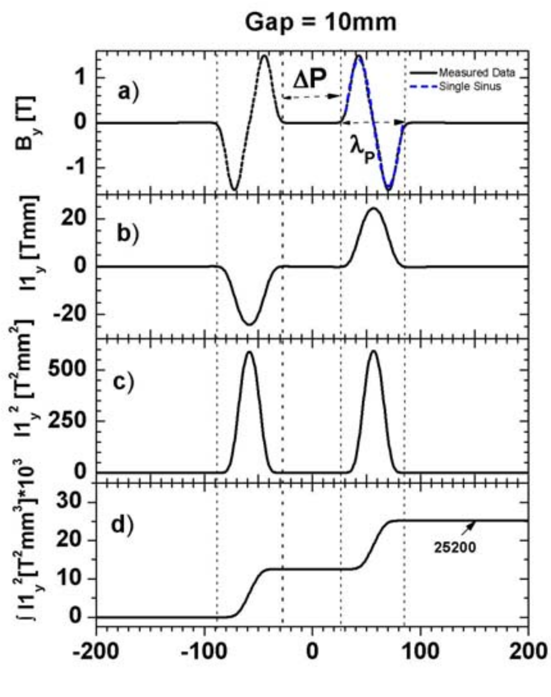

Figure 8: Measured field profiles and derived properties as function of z. The gap of the phase shifter was10mm. a) B_y field distribution, a single sinusoid is fitted to the positive part of the field. b) first field integral, c) The square of the first field integral. d) Phase integral, the value at the end amounts to 25200T^2mm^3.

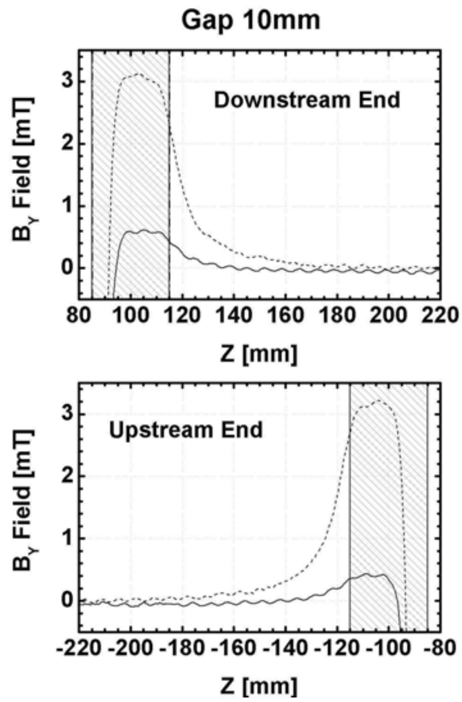

Figure 9: Fringe field outside the phase shifter. Note the expanded scale as compared to Fig. 8a). The Phase shifter extends from Z=- 115 to 115mm. The position of the iron yoke is indicated by the hatched area. The dashed curve shows the effect of remanent magnetization in the iron during the optimization, the full curves shows the final state.

It is seen in Fig 8b) and c) as well, that well behind the phase shifter the field integral is very small. Finally Fig 8d) shows the evolution of the Phase Integral. The maximum value after the phase shifter amounts to 25200 T^2mm^3, which meets the requirement in Table 1 but nevertheless is 10% smaller than predicted by Eq. (9). The explanation is the presence of a 3rd field harmonic, which reduces the field integral but not the peak field. This effect is known for hybrid field configurations.

Fig. 9 shows the magnetic fringe field outside of the phase shifter. The scale is expanded by a factor 300 as compared to Fig 8a). The gap is again 10mm. The two curves correspond to different pre-treatments, which are explained below. The phase shifter extends from -115 to 115 mm. Only the outside regions down- and upstream are shown. The hatched areas mark the locations of the 30mm thick iron yokes. At Z=±71.25 mm, only 13.75 mm away from the yoke there are the locations of the negative poles, where the field is -1.5T. Under the yoke, however, within the length of the yoke gap of about 10mm the field approaches to levels of several Millitesla. Outside it fades off further. The two curves show the effect of remanent yoke magnetization, which was observed in the measurements. In the data it was easily visible in the first field integral, which had an initial nonzero value in the -0.1Tmm and was completely independent of the gap. In order to get the yoke demagnetized a temporary coil was wound around the whole phase shifter. By applying about ±3200 Ampere-turns the magnetization could be flipped and by gradually reducing the amplitude the yoke was de-magnetized. However, a perfect zero field under the yoke was very difficult to obtain. The full curves in Fig. 9 show the best effort obtained in this way. There is still a field of about 0.4mT under the center of the yoke. For comparison the dashed curve shows an intermediate state.

After demagnetization gap dependent measurements were made they are shown in Fig. 10. Measured data points are indicated by symbols. Fig. 10a) shows the gap dependence of the vertical peak field, Fig. 10b) that of its total first field integral and Fig. 10c) the gap dependence of the total Phase Integral, see Eq. (6). Peak field and Phase Integral follow an exponential gap dependence of the form $y= a\ exp(b\ g + c\ g^2)$. Least square fits are shown by the dashed lines and the resulting parameters in the boxes in Fig.10. The total first field integral is very small, well within±0.01Tmm, for any gap as can be seen in Fig. 10b). This is, however, slightly above the required ±0.004Tmm, see table 1 and needs some slight improvement in future.

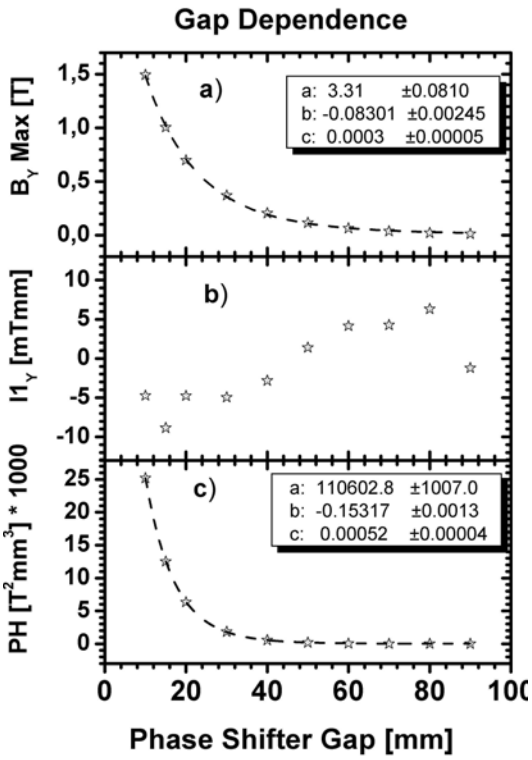

Figure 10: **Peak field, 1st Field Integral and Phase integral as a function of the gap. Measurements are indicated by symbols. The dashed lines are fits to the data of the form:** *y= a exp(b g + c g²)*

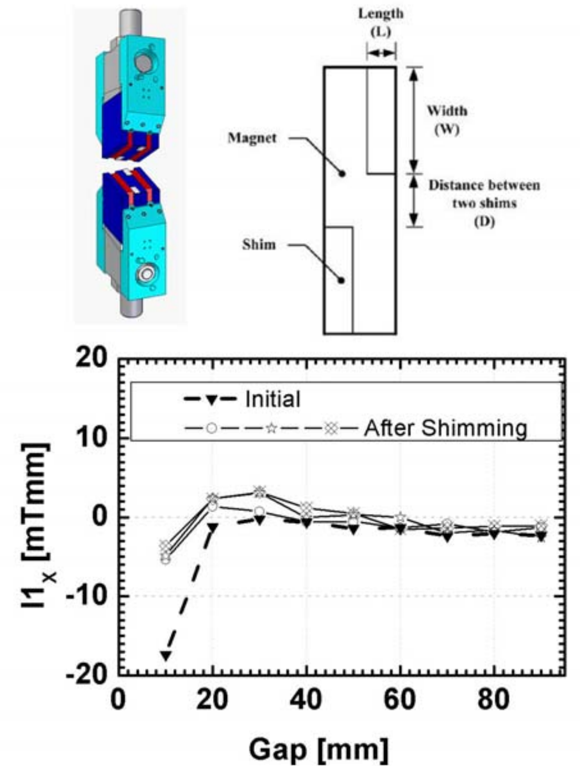

Figure 11: Results of horizontal shimming. Top: Geometry and application of the shims. Bottom: Gap dependence of the horizontal field integral of B_x befor (full triangle) and after applying shims (open symbols). The three different scans illustrate the accuracy of the measurements.

Total horizontal field integrals are shown in Fig. 11, bottom. The full triangles show the initial state. Here the maximum field integral error is about 0.017Tmm. This is already a quite small number. However, a further reduction was needed in order to reduce the influence of field errors and to meet the specs shown in table 1.

Iron shims with the geometry sketched in the upper part of Fig. 11 were systematically investigated. Length (L), Width (W), Distance (D) and the thickness of the shims were varied and the gap dependence of the horizontal field integral was measured. Optimum shim dimensions, which minimize the gap dependence of the horizontal first field integral, were found to be: 8mm × 3mm × 0.1mm × 2mm (Length ×Width × Thickness × Distance). The final results and their reproducibility are shown as Figure 11. As compared to the initial values there is a reduction by more than a factor 3.

5. Discussion and Summary

Using the results presented so far the operation of this device in an undulator system and the limitations are discussed.

The total Phase Integral is a function of the phase shifter gap, g_P, so $PI(g_P)$. In the same fashion, the undulator gap, g_u, determines the radiation wavelength via the K-parameter, $K_U(g_U)$. For both functions there are good approximation using the exponential coefficients, see Fig. 10 and ref [14].

Implicit solutions of Eq. (11) i.e. the calculation of the phase shifter gap g_P for a given undulator gap g_U for different Phase Numbers ν and intersection length L are shown in the right part of Fig. 12. for the SASE2 and SASE3 undulator systems of the XFEL. The dashed curves correspond to odd, the full curves to even field geometry. The vertical dotted line indicates the short wavelength design limits. For orientation wavelength scales are given at the top of the figures as well.

For a given ν the phase shifter can be used only for radiation wavelengths larger than $L/\nu\gamma^2$. For tuning over a more extended wavelength range two alternatives exist: The first is to jump to a higher ν incremented by a multiple of 2. In this way the required Phase Integral can be kept moderate. There is no limit on achievable short wavelengths by Phase number hopping. However, there is a substantial gap change needed for the Phase Shifter each time the radiation wavelength approaches $L/\nu\gamma^2$. This prevents continuous scanning over the whole design range of the undulator system. The second alternative is to choose ν large enough for the whole wavelength range. This requires a larger available tuning range for the Phase Integrals, but there are no jumps and continuous

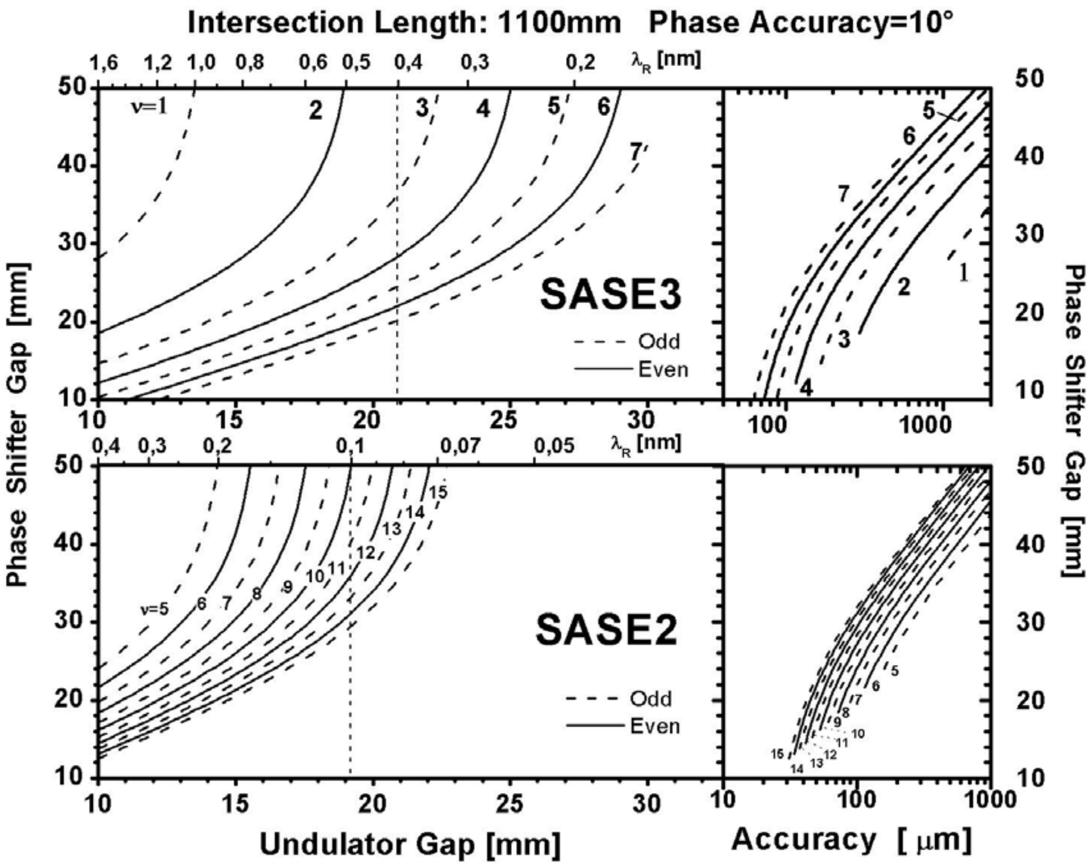

Figure 12 Tuning curves for the phase shifter for the SASE 2 and SASE3 Undulator Systems of the XFEL. The graphs on the right show the required gap precision of the phase shifter for to control the phase within ±10°

scanning is possible.

This is illustrated for SASE3, which has the toughest requirements on Phase Integral, see Fig. 12.. Assuming an odd field geometry and starting with ν=1 the phase shifter can only be tuned for wavelengths larger than about 1nm. This limit is reached at a SASE3 gap of 13.5mm. In order to change to ν=3 the phase shifter gap needs to be changed from about 50 to 19.3mm. With ν=3 the 1.6nm wavelength limit can be safely reached. Using ν=3 from the beginning would require an initial phase shifter gap of 14.6mm. As can be seen from the data shown in Fig. 12 ν=5 is the limit for SASE3 parameters. For the cases with even field geometry namely ν=2 and 4 the situation is similar. For Phase Numbers larger than 5 the Phase Integral is outside the designed gap range and cannot be accessed anymore.

The situation is somewhat different for SASE2. For continuous tune-ability from 0.1 to 0.4nm without jumps ν≥10 has to be chosen. The strength is sufficient even for ν=15 or higher. But there is, however, another aspect: The phase integral and its derivative with respect to gap decreases exponentially with the gap (see Fig.10). Consequently the accuracy requirement decreases inversely and become more challenging. The resulting accuracy requirements for a phase error of ±10° are shown in the right sections of Fig.12. A logarithmic scale is used in order to visualize the large variation due to the exponential behavior. It is seen that for SASE3 and ν=3 the accuracy may well be above ±100 μm. For SASE2, however, ν needs to be 10 or larger in order to cover the whole the tuning range from 0.1 to 0.4nm. Here at the short wavelengths the gap control accuracy needs to be ±50μm. This is touching the limits but it is still within the capabilities of the system as demonstrated in Fig. 7. It is seen in Fig 12 that ν should be chosen as small as the tuning range allows in order to keep the accuracy

requirement as moderate as possible. In order to improve gap accuracy there are two alternatives: The first is to apply a backlash correction, i.e. move to positions always from one side. This is justified by the very good reproducibility of ±1-2µm observed in the measurements shown in Fig.7 and is easy to implement. However it only works in one direction.
The second is to use an encoder system, which measures the true phase shifter gap and is included in the closed loop feedback of the phase shifter gap control. Any accuracy can be obtained at an appropriate extra effort.
A complication, however, is the proximity to the electron beam since encoders are prone to radiation damage. With an encoder the phase shifter gap can be accessed from any direction with high accuracy and without restrictions.
From the standpoint of operation safety and operational simplicity, however, the first alternative is clearly preferable. If the hysteresis loops in Fig 7 are approximated by an average curve they contain an intrinsic position uncertainty of about ±50µm. This would allow for sufficient positioning accuracy for SASE3 anyhow. Also most of the operational range of SASE2 can be safely covered. Only close to 0.4nm at smallest gaps accuracy touches the limits.
The gap tuning curves presented in this paper are fully based on magnetic measurements. They are made in a magnetic lab prior to installation. However, once an undulator system is installed in the XFEL other methods have to be applied. On way could be a photon diagnostic system as described in ref. [16]. It was shown that the photon energy spectrum of the emitted spontaneous synchrotron radiation intensity of two adjacent undulator segments is quite sensitive to the phasing. So this effect can be used to measure the phase setting as a function of the undulator gap. This is only one of the in situ performance checks of an undulator system, which can be done with such a system. More are proposed in ref [16].

6. Summary

A novel phase shifter based on permanent magnets for the use in the European XFEL project has been developed and tested. The maximum measured strength was found to be sufficient for the use as a standard device in the XFEL. Continuous phase adjustment for wavelength tuning in the range 0.1 to 0.4nm for the SASE2 and 0.4 to 1.6nm for the SASE3 undulator systems of the XFEL is possible.
The basic magnetic design principle is based on symmetry and was shown to work well. Field integral errors in both directions cancel almost perfectly. Using suitable shims these properties could be further improved and tuned to very low limits. The magnetic results in both directions touch the resolution limits of magnetic measurements.
Using a motion control system without direct measurement of the gap and neglecting mechanical hysteresis provides an accuracy of ±50µm, which is sufficient for all cases. However it touches the limits for SASE2 when operated at 0.4nm.
The remanence in the iron yoke needs special attention. Demagnetization as described above is only considered an emergency solution since complete demagnetization could not be obtained as was shown in the discussion of Fig.9. The magnetic treatment of the iron for the zero potential yoke needs special attention. It is very important to make sure that there is no remanent magnetization, which leads to a field between the yokes leading to a constant field integral contribution independent of the gap. Thermal annealing at about 850°C provides both complete thermal demagnetization and optimum properties at low excitation. With this treatment the coercive field, H_C, can be as low as 60-70A/m. Without annealing, however, H_C depends on the mechanical history of the part like machining or mechanical deformation. In these cases H_C can be several times higher.

7. Acknowledgements

The authors would like to thank U. Englisch, P. Neumann, A. Schoeps, M. Tischer and T. Vielitz for support and many helpful discussions.

8. REFERENCES

[1] M. Altarelli, Editor, The European X-Ray Free Electron Laser Technical Design Report, ISBN 3-935702-17-5
[2] A. M. Kondratenko and E. L. Saldin, Part. Accel. 10, 207 (1980)
[3] R. Bonifacio, C. Pellegrini, and L. M. Narducci, Opt. Commum. 50, 373 (1984)
[4] B. Faatz, J. Pflueger, Y.M. Nikitina TESLA-FEL 96-13 (1996)
[5] E. Gluskin, N.A. Vinokurov, G. Decker, R.J. Dejus, P. Emma, P. Illinski, L. Moog, H.D. Nuhn, I. Vasserman, Nucl. Instr. and Meth. A475, (2001) 323
[6] G. Materlik, T. Tschentscher editors,TESLA Technical Design Report Part V, X-Ray Free electron Laser, ISBN 3-935702-04-3, DESY 2001-011, TESLA-FEL 2001-05
[7] J. Pflueger, M. Tischer, TESLA-FEL report 2000-08, DESY, Hamburg (2000), http://flash.desy.de/reports_publications/tesla_fel_reports/

[8] J. Pflüger, Proceedings of the FEL 2005, August 21-26. Stanford USA
[9] H. Lu, M. Wang, J. Zhuang, D. Wang, J. Pflueger, P. Neumann, M. Rueter, M. Tischer, T. Vielitz, Proceedings of the Free Electron Laser Conference FEL2008, Aug. 24-29, 2008, Geongju, Korea
[10] R. P. Walker Nucl. Instr. And Meth. A335, (1993) 328
[11] K. Halbach, R.F. Holsinger, Particle Accelerators 7(4), 213-222 (1976). The 2008 version can be downloaded from: http://laacg1.lanl.gov/laacg/services/download_sf.phtml
[12] S. Reiche, GENESIS 1.3 Nucl. Instr. and Meth. A429, (1999), 243
[13] Y. Li, B. Faatz, J. Pflueger, Phys. Rev ST-AB 11, 100701 (2008)
[14] P. Elleaume, J. Chavanne, B. Faatz, Nucl. Instr. and Meth. A445 (2000), 503
[15] P. Elleaume, O. Chubar, J. Chavanne, Proc. IEEE PAC-97. 9P27, 3509-3511
[16] M. Tischer, U. Hahn, J. Pflueger, H. Schulte-Schrepping, P. Illinski, Nucl. Instr. and Meth. A483 (2002) 418

9. Appendix: Proposed Improvements for the Pre- Series Prototypes

Quite some practical experience was gained with the first prototype. Its main purpose was to study the proof of principle and to demonstrate that the tough field integral tolerances can be achieved. For this prototype the required production of 92 of such devices needed for the XFEL did not play the dominant role.
Nevertheless as demonstrated in this paper the principle proved very successful and will be used for the XFEL phase shifters. In this appendix points and facts are reported, which came up during commissioning and during the magnetic measurements and tuning. Not all of them were explicitly mentioned in the report. Some of these were purely technical and/or might have some impact on the cost of future systems.
So they might be used to simplify the design and thus help to reduce cost or they improve device properties and operational reliability.
A summary of all points is given below:

- **Magnetic treatment of the iron yoke**
  The magnetic treatment of the yoke material is of paramount importance. This includes proper magnetic annealing. Magnetic annealing was NOT done on the yoke of the prototype. The demagnetization procedures described in the report are emergency procedures and require additional effort and time. Moreover demagnetization was not easy as demonstrated in Fig.9 of the report.
- **Magnetic connection between top and bottom yoke**
  A massive magnetic soft iron connection between the upper and lower yokes is recommended. It acts like a magnetic short circuit and prevents that a magnetic potential is built up between the upper and lower half of the yoke. Since the iron yokes are kept fixed, this connection can easily feasible.
- **Simplification of geometry**
  As compared to the prototype the geometry of the iron yokes can be simplified without compromise on performance. The iron cross section can be reduced. A yoke thickness of 15-20mm is certainly sufficient. This would help to reduce cost. However the separation of the upstream and downstream halves, which determines ΔP, see Fig 1, 8 should be kept constant.
- **Maximum gap**
  The maximum gap of the prototype was about 130mm. It might reduced less than half the value and limited to 50-60mm. This will reduce the size of the iron yoke significantly and reduce cost.
- **Reduction of mechanical hysteresis**
  The mechanical hysteresis seen in Fig. 7 in the mechanical system is caused by friction and backlash. The system is quite accurate. Stiffer supports and lower friction will help to reduce mechanical hysteresis. There should be a small well controlled air gap between the magnet packages and the iron yoke of about 0.1-0.2mm so that easy sliding is possible. The sliding surfaces of the yoke should be suitably smooth machined surface i.e. at least an N8 surface with 3.2μm RMS roughness or better N7 (1.6μm). Some greasing of these surfaces should be considered.
- **Spindle, self locking gear box, electronic brake**
  The drive chain consisting of the spindle, gearbox and motor with an electronic brake can be simplified. The pitch should be reduced. Eventually the ball screws can be replaced. However care is to be taken not to compromise too much on accuracy. A self locking element should be included in the drive chain such as a worm gear with some friction. This would provide some inherent operational safety and prevent the magnets from moving if brakes are open and motor is not powered. Eventually the brake is not needed anymore. This would also help reducing cost.
- **Adjustable hard stops**
  An adjustable hard stop, which limits the low gap to 10-11mm is required. This is completely missing in the prototype

- **Adjustable limit switches**
  Suitable limit switches which can be easily and precisely adjusted, should be foreseen at the upper and lower gap position. A separate initiator is eventually needed for initializing the control system. However, the option of using absolute multi-turn encoders on the drive motor should be checked. It would eliminate the need for initialization and always provide an absolute gap value even after power failure. The undulator systems use this kind of motor.
- **Pole height tuning and tilting**
  In order to make full advantage of pole height tuning and tilt procedures suitable access to the adjustment screws of the poles has to be provided. This was not the case for the prototype and would further improve the error correction and introduce capabilities, which go beyond those described in this paper. For example fo the PETRA III devices pole tilting is now routinely used to tune horizontal field errors without using any shims. In this sense the results of this paper are only upper limits, which might be even better in future.